Optical and Quantum Electronics (2022) 54:827
https://doi.org/10.1007/s11082-022-04160-2

Computational investigation of all-optical NOR logic operation using carrier reservoir semiconductor optical amplifiers at 120 Gb/s

Amer Kotb[1,2] · **Kyriakos E. Zoiros**[3] · **Wei Li**[1]

Received: 16 August 2021 / Accepted: 1 September 2022 / Published online: 19 October 2022
© The Author(s), under exclusive licence to Springer Science+Business Media, LLC, part of Springer Nature 2022

Abstract
The carrier reservoir semiconductor optical amplifier (CR-SOA) is considered an appealing alternative for overcoming the slow gain response of the conventional SOA and supporting all-optical (AO) logic operations at enhanced data rates. In this paper, CR-SOAs are employed in the Mach-Zehnder interferometer (MZI) to theoretically investigate and demonstrate, for the first time, the AO NOT-OR (NOR) logic operation at 120 Gb/s on-off keying of return-to-zero pulse format. To confirm the potential and suitability of using CR-SOAs in this context, we compare the performance of the logic scheme against that with the conventional SOAs by examining and assessing the dependence of the NOR gate's quality factor (Q-factor) on various key operating parameters, which include the input power, the injection current, and the data rate in the presence of noise incurred by amplified spontaneous emission for more realistic calculations. The results show that owing to the CR-SOAs' faster dynamic response, the CR-SOAs-MZI is a favorable technological option for implementing the NOR logic gate at 120 Gb/s, since it achieves a Q-factor value of 14 and accordingly high quality correct operation, as opposed to the unacceptable value of 4.4 when utilizing for the same purpose the corresponding switching module with conventional SOAs.

Keywords All-optical NOR logic operation · Carrier reservoir semiconductor optical amplifier · Mach-Zehnder interferometer · Quality factor

✉ Amer Kotb
amer@ciomp.ac.cn

✉ Wei Li
weili1@ciomp.ac.cn

[1] GPL, State Key Laboratory of Applied Optics, Changchun Institute of Optics, Fine Mechanics, and Physics, Chinese Academy of Sciences, 130033 Changchun, China

[2] Department of Physics, Faculty of Science, University of Fayoum, 63514 Fayoum, Egypt

[3] Lightwave Communications Research Group, Department of Electrical and Computer Engineering, School of Engineering, Democritus University of Thrace, 67100 Xanthi, Greece

1 Introduction

The NOT-NOR (NOR) logic gate is a universal gate that is used to create any Boolean function (Xu et al. 2008), build combinational logic circuits (Jung et al. 2008), manage packet contention (Scaffardi et al. 2007), and monitor bit error rate (Chan et al. 2003). For this purpose, it is equally important in the optical domain, where it is thus highly desirable to be implemented. To this aim, the semiconductor optical amplifier (SOA) is as an attractive nonlinear element that owing to properties such as the low power consumption, the low-cost factor, the large bandwidth, the compact size, and the affordable integration with other optoelectronic devices (Kotb et al. 2018), has extensively been used for designing all-optical (AO) logic gates, like the NOR at different data rates (Kotb et al. 2018; El-Saeed et al. 2016; Mehra et al. 2013; Sun et al. 2007; Xu et al. 2006; Kotb 2013a, b, 2015; Kotb and Guo 2020a, b; Dimitriadou and Zoiros 2012; Dutta and Wang 2013). However, the SOA operation beyond data rates of the order of 100 Gb/s is hindered by its inherently slow gain response. Thus, finding other alternative active nonlinear elements that can overcome this limitation of conventional SOAs is very crucial. Recently, the carrier reservoir SOA (CR-SOA) has been employed to implement AO XOR, AND, OR, NAND, and XNOR logic gates (Kotb et al. 2021a, b, c; Kotb 2021). In this paper, we extend, complete, and generalize our prior work on AO gates using CR-SOAs (Kotb et al. 2021a, b, c; Kotb 2021) by computationally treating the AO NOR logic gate at 120 Gb/s on-off keying of return-to-zero (RZ-OOK) pulse format. For this purpose, two symmetrical CR-SOAs are incorporated in the Mach-Zehnder interferometer (MZI), which is the prominent technological candidate for realizing AO switching functionalities (Kotb 2021). The dependence of the NOR gate's quality factor (Q-factor) on various key operating parameters, such as the input power, the injection bias current, and the data rate is examined by comparison between CR-SOAs- and conventional SOAs-assisted MZI. The effect of amplified spontaneous emission (ASE) noise on the Q-factor for both CR-SOA and conventional SOA is also taken into account for more realistic calculations.

2 AO NOR logic gate

2.1 Principle of operation

A NOR logic gate gives '1' at its output only when both of its inputs are '0', else it produces a '0' for any other input binary combination. The schematic diagram of the NOR diagram build using as a core module the CR-SOAs-assisted MZI is shown in Fig. 1, together with the corresponding truth table.

The circuit shown in Fig. 1 is used to achieve the AO NOR operation with either CR-SOAs or conventional SOAs embedded in the MZI. Via wavelength-selective couplers (WSCs), input data signals A and B at two different wavelengths λ_A and λ_B, respectively, are combined and injected into the upper arm of the CR-SOAs-MZI at port 1 (i.e. CR-SOA1), while a signal of repetitive pulses, i.e. a clock signal (Clk) at λ_{Clk}, enters the lower arm of the CR-SOAs-MZI at port 2 (i.e. CR-SOA2). Concurrently, a continuous wave (CW) beam at λ_{CW} is divided by a 3 dB optical coupler (OC) into two halves, which enter distinctly CR-SOA1 and CR-SOA2 through the CR-SOAs-MZI middle arm at port 3. The binary con-

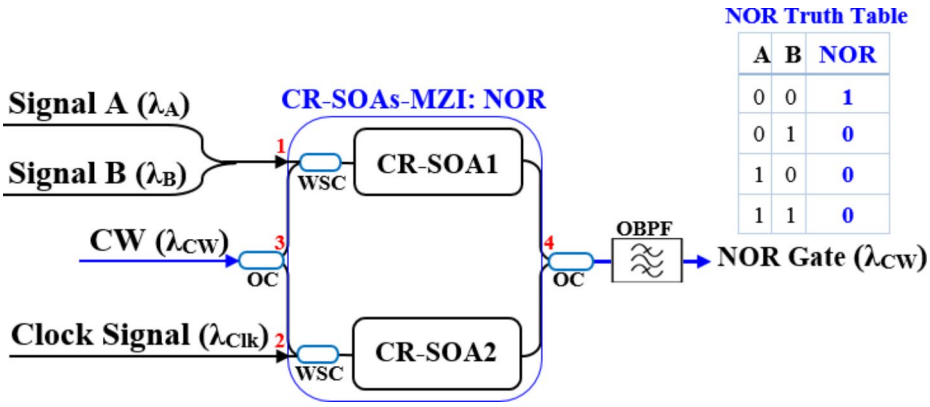

Fig. 1 Schematic diagram of NOR gate build using CR-SOAs-assisted MZI and corresponding truth table. CW: continuous wave. OC: 3 dB optical coupler. WSC: wavelength-selective coupler. OBPF: optical bandpass filter

tent of signals A and B modulates the gain and phase of the CW split constituents through the CR-SOAs cross-gain modulation (XGM) and cross-phase modulation (XPM) nonlinear effects. When light of two distinct wavelengths, i.e. a pump and a probe, is fed into the AR, XGM manifests as a result of gain saturation in (CR)-SOA. The available optical gain is allocated between the two wavelengths depending on their relative photon densities when (CR)-SOA is operated under gain saturation conditions. Changes in the pump power have an inverse influence on the probe gain, resulting in data transfer required for logic gate realization. When two optical signals are injected into the (CR)-SOA at the same time, the carrier density dynamic perturbation alters not only the optical gain but also the refractive index, which through XPM induces a phase change on the probe signal and thus results in data switching. When at least one of A or B is present, i.e. A = '1' and B = '0', A = '0' and 'B = '1', or A = '1' and B = '1', CR-SOA1 becomes saturated by their combination. Under the simultaneous presence of all 1's contained in the Clk signal, CR-SOA2 is also driven into saturation. As a consequence, the CW components inserted into CR-SOA1 and CR-SOA2 encounter identical dynamic properties, so that they interfere destructively when recombined at the output OC, thus resulting in a logical '0'. On the contrary, when both A and B are '0', all 1's in the Clk signal break the MZI balance so that the CW beam replicas interfere constructively resulting in a logical '1' at the output. The output of this procedure is imprinted on the outgoing CW beam at λ_{CW} selected by an optical bandpass filter (OBPF).

2.2 Modeling

In CR-SOA, the CR layer is grown in the vicinity of the active region (AR), as shown in Fig. 2 (Dutta and Wang 2013; Kotb et al. 2021a, b, c; Kotb 2021). The ultrafast transition is in the range between 0.5 and 5 ps from the filled CR to the depleted AR.

The active region (AR) layer in CR-SOA has a greater bandgap than the CR layer. Carriers in both AR and CR begin to fill the available states when an injection current is applied. At low current, the AR has a larger carrier density than the CR. As the injection current is raised, the CR accumulates enough carriers to function as a reservoir of supplied carriers.

Fig. 2 Band diagram of CR-SOA

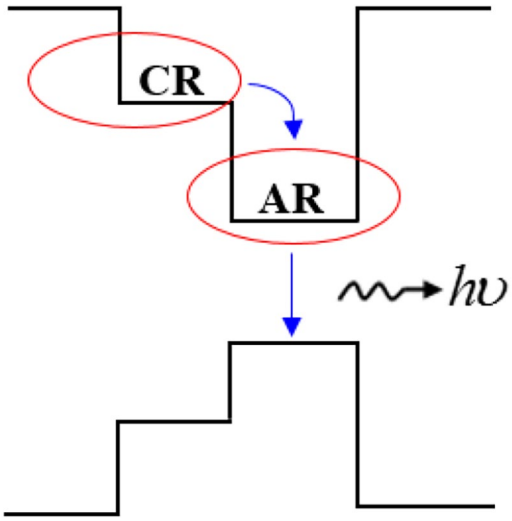

The incident photons are driven into the AR by the stimulation emission process and collide with electrons, creating photons. The carriers depleted in the AR by an intensive signal in the active area are immediately replaced by the heavily filled CR's. The CR-SOA gain and phase response can be accelerated by transitioning from the CR to the AR in a few picoseconds (Dutta and Wang 2013). At high intensities, the intraband nonlinear effects of the carrier heating (CH) and spectral hole burning (SHB) manifest inside CR-SOA at an ultrashort time scale of subpicoseconds. The influence of CH and SHB should be taken into account for accurately modeling the CR-SOA behavior. Therefore, the nonlinear effect of carrier recombination between the AR and CR levels as well as the intraband nonlinear effects of both CH and SHB are considered through the first-order differential rate equations for each CR-SOA, i.e. (Dutta and Wang 2013; Kotb et al. 2021a, b, c; Kotb 2021):

$$\frac{dh_{AR}(t)}{dt} = \frac{h_{CR}(t) - h_{AR}(t)}{\tau_t(1+\eta)} + \frac{\eta\, h_0}{\tau_c(1+\eta)} - \frac{h_{AR}(t)}{\tau_c} - (exp\,[h_{AR}(t) + h_{CH}(t) + h_{SHB}(t)] - 1)\,\frac{P_{in}(t)}{E_{sat}} \quad (1)$$

$$\frac{dh_{CR}(t)}{dt} = -\frac{\eta(h_{CR}(t) - h_{AR}(t)}{\tau_t(1+\eta)} + \frac{h_0 - h_{CR}(t)}{\tau_c(1+\eta)} - \frac{h_{CR}(t)}{\tau_c} \quad (2)$$

$$\frac{dh_{CH}(t)}{dt} = -\frac{h_{CH}(t)}{\tau_{CH}} - \frac{\varepsilon_{CH}}{\tau_{CH}}(exp\,[h_{AR}(t) + h_{CH}(t) + h_{SHB}(t)] - 1)\,P_{in}(t) \quad (3)$$

$$\frac{dh_{SHB}(t)}{dt} = -\frac{h_{SHB}(t)}{\tau_{SHB}} - \frac{\varepsilon_{SHB}}{\tau_{SHB}}(exp\,[h_{AR}(t) + h_{CH}(t) + h_{SHB}(t)] - 1)\,P_{in}(t) - \frac{dh_{AR}(t)}{dt} - \frac{dh_{CH}(t)}{dt} \quad (4)$$

where the different functions 'h' represent the CR-SOA gain integrated over the CR-SOA length for the carrier recombination between AR and CR, CH, and SHB. τ_t and τ_c are the transition times from the CR layer to the AR layer and the carrier lifetime in both AR and CR, respectively. η is the population inversion factor given by $\eta = N_{AR}/N_{CR}$ (Dutta and

Wang 2013), where N_{AR} and N_{CR} are the carrier densities in AR and CR, respectively. $h_0 = \log[G_0]$, where G_0 is the unsaturated power gain linked to the CR-SOA parameters by $G_0 = \alpha\Gamma\ (I\tau_c/eV - N_{tr})\ L$ (Dutta and Wang 2013), where α is the differential gain, Γ is the optical confinement factor, I is the injection current, e is the electron charge, V is the AR volume, N_{tr} is the transparency carrier density, and L is the length of the AR. The quantity N_{tr} is defined as the carrier density at which the optical gain is zero. The typical value of N_{tr} for InGaAsP amplifiers is between 1.0 and 1.5×10^{18} cm^3 (Dutta and Wang 2013). $E_{sat} = P_{sat}\ \tau_c = wd\hbar\omega_0/\alpha\Gamma$ (Dutta and Wang 2013), where E_{sat} is the saturation energy, P_{sat} is the saturation power, w & d are the width and thickens of the AR, respectively, ħ is Planck's constant divided by 2π, and ω_0 is the central optical frequency. τ_{CH} and τ_{SHB} are the temperature relaxation rates for CH and SHB, respectively. ε_{CH} and ε_{SHB} are the nonlinear gain compression factors for CH and SHB, respectively. The time-dependent differential equations for the conventional SOA and the related equations are presented in detail in Chap. 9 of Ref. (Dutta and Wang 2013). $P_{in}(t)$ is the time-dependent input power of signals A, B, and Clk, assumed to comprise Gaussian-shaped RZ-OOK pulses, i.e. (Kotb 2015; Kotb and Guo 2020a, b):

$$P_{A,B,Clk}(t) \equiv P_{in}(t) = \sum_{n=1}^{N} a_{n(A,B,Clk)} \frac{2\sqrt{\ln[2]}\,E_0}{\sqrt{\pi}\,\tau_{FWHM}} \exp\left[-\frac{4\ln[2](t - nT)^2}{\tau_{FWHM}^2}\right] \quad (5)$$

where $\alpha_{n(A,B)}$ = '1' or '0' and $\alpha_{n(clk)}$ = '1', E_0 is the pulse energy, τ_{FWHM} is the pulse width (FWHM: full-wave at half-maximum), N is the length of the pseudorandom binary sequence (PRBS) of each data A, B, taken herein as $N = 2^7\text{-}1$ (Kotb et al. 2018; Kotb 2015; Kotb and Guo 2020a, b), and T is the bit period defined as the inverse of the data rate in Gb/s (i.e. T = 1000/data rate).

The input optical powers entering CR-SOA1 and CR-SOA2 as shown in Fig. 1 are, respectively, expressed by (Sun et al. 2007):

$$P_{in,\,CR-SOA_1}(t) = P_A(t) + P_B(t) + 0.5\,P_{CW} \quad (6)$$

$$P_{in,\,CR-SOA_2}(t) = P_{Clk}(t) + 0.5\,P_{CW} \quad (7)$$

where coefficient '0.5' denotes the divided by the 3 dB OC parts of the CW input coupled into the MZI interferometer middle arm. Then, the NOR power at the CR-SOAs-MZI output is given by (Kotb 2013a, b; Kotb and Guo 2020a, b):

$$P_{NOR}(t) = 0.25\,P_{CW}\left(G_{CR-SOA_1}(t) + G_{CR-SOA_2}(t) - 2\sqrt{G_{CR-SOA_1}(t)\,G_{CR-SOA_2}(t)}\cos\left[\Phi_{CR-SOA_1}(t) - \Phi_{CR-SOA_2}(t)\right]\right) \quad (8)$$

where $G_{CR\text{-}SOA1,2}(t)$ and $\Phi_{CR\text{-}SOA1,2}(t)$ are, respectively, the gains and phase shifts of the CR-SOA1 and CR-SOA2 induced on the CW beam components traveling through these devices. The total output gain of each CR-SOA, including the interband as well as intraband nonlinear effects, is described by (Dutta and Wang 2013):

$$G_{CR-SOA_i}(t) = exp\left[h_{AR}(t) + h_{CH}(t) + h_{SHB}(t)\right],\ i = 1,\ 2 \quad (9)$$

Table 1 NOR default operating parameters (Kotb et al. 2018, 2021a, b, c; El-Saeed et al. 2016; Mehra et al. 2013; Sun et al. 2007; Xu et al. 2006; Kotb 2013a, b, 2015, 2021; Kotb and Guo 2020a, b; Dimitriadou and Zoiros 2012; Dutta and Wang 2013)

Symbol	Definition	Value	Unit
$\mathbf{E_0}$	Pulse energy	0.8	pJ
$\boldsymbol{\tau_{FWHM}}$	Pulse width	1	ps
T	Bit period	8.33	ps
N	PRBS length	127	-
$\boldsymbol{\lambda_A}$	Wavelength of signal A	1549.2	nm
$\boldsymbol{\lambda_B}$	Wavelength of signal B	1535	nm
$\boldsymbol{\lambda_{Clk}}$	Wavelength of Clk	1555	nm
$\boldsymbol{\lambda_{CW}}$	Wavelength of CW	1550	nm
I	Injection current	200	mA
$\mathbf{P_{sat}}$	Saturation power	30	mW
$\boldsymbol{\tau_c}$	Carrier lifetime	200	ps
$\boldsymbol{\tau_t}$	Transition lifetime from CR to AR	5	ps
sη	Population inversion factor	0.3	-
α	α-factor	5	-
$\boldsymbol{\alpha_{CH}}$	Linewidth enhancement factor for CH	1	-
$\boldsymbol{\alpha_{SHB}}$	Linewidth enhancement factor for SHB	0	-
$\boldsymbol{\varepsilon_{CH}}$	Nonlinear gain compression factor for CH	0.2	W^{-1}
$\boldsymbol{\varepsilon_{SHB}}$	Nonlinear gain compression factor for SHB	0.2	W^{-1}
$\boldsymbol{\tau_{CH}}$	Temperature relaxation rate	0.3	-
$\boldsymbol{\tau_{SHB}}$	Carrier-carrier scattering rate	0.1	ps
Γ	Optical confinement factor	0.3	-
a	Differential gain	10^{-16}	- cm^2
$\mathbf{N_{tr}}$	Transparency carrier density	10^{18}	cm^{-3}
L	Length of AR	0.5	mm
d	Thickness of AR	0.3	µm
w	Width of AR	3	µm
$\mathbf{G_0}$	Unsaturated power gain	30	dB
$\mathbf{N_{SP}}$	Spontaneous emission factor	2	-
υ	Central optical frequency	193.55	THz
$\mathbf{B_0}$	Optical bandwidth	2	nm
h	Planck's constant	6.63×10^{-34}	J.s

The total phase shift induced on the CW beam launched into each CR-SOA is given by (Dutta and Wang 2013):

$$\Phi_{CR-SOA_i}(t) \;=\; -0.5\,(\alpha\, h_{AR}(t) \;+\; \alpha_{CH}\, h_{CH}(t)),\; i = 1, 2 \tag{10}$$

where α symbolizes the traditional linewidth enhancement factor (i.e. α-factor) and α_{CH} is the linewidth enhancement factor for CH. As it is implied from Eq. (10), the contribution of the linewidth enhancement factor for SHB (α_{SHB}) is null, i.e. $\alpha_{SHB}=0$ (Kotb 2013a, b, 2021; Kotb and Guo 2020a, b; Dutta and Wang 2013; Kotb et al. 2021a, b, c).

The time-domain Eqs. (1)-(10) have been combined and solved using Adams numerical method run in Wolfram Mathematica®. For a fair performance comparison, the default operating parameters cited in Table 1 (Kotb et al. 2018, 2021a, b, c; El-Saeed et al. 2016;

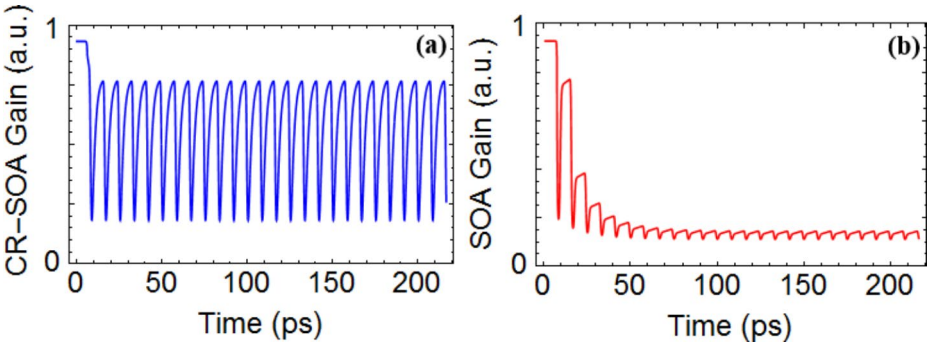

Fig. 3 Comparison of gain response at 120 Gb/s for (**a**) CR-SOA and (**b**) conventional SOA

Mehra et al. 2013; Sun et al. 2007; Xu et al. 2006; Kotb 2013a, b, 2015, 2021; Kotb and Guo 2020a, b; Dimitriadou and Zoiros 2012; Dutta and Wang 2013) are used for both CR-SOA and conventional SOA.

A comparison of the temporal gain response between the CR-SOA and the conventional SOA at 120 Gb/s is shown in Fig. 3(a) and (b), respectively. From this figure, it is apparent that because of the shorter transition time in the 0.5 to 5 ps range from the CR to the AR in the CR-SOA, the latter can be operated, and hence exploited for switching, at faster rates with uniform gain variation, as opposed to the conventional SOA, which suffers from irregular gain variation.

The waveforms of the input and output signals of CR-SOA1 and CR-SOA2 at 120 Gb/s are depicted in Fig. 4. According to Eq. (6), the form of $P_{in,\ CR\text{-}SOA1}(t)$ is the logic combination of A = '0', B = '1' and A = '1', B = '0', which are simultaneously launched into CR-SOA1. The CW probe beams from both CR-SOA1 and CR-SOA2 interfere at the MZI output, and the NOR output gate is realized.

We simulate the signal gain as a function of the wavelength from 1350 nm up to 1600 nm for both CR-SOAs and SOAs at 120 Gb/s, as presented in Fig. 5. The CR-SOA provides higher gain, which allows for more efficient all-optical switching, across the whole examined spectral span, including the 1550 nm window which is of particular interest for optical telecommunications.

The 2^7-1 PRBS data streams A and B and the corresponding output of the NOR gate for CR-SOAs- and SOAs-based MZI at 120 Gb/s are shown in Fig. 6. Figure 7 shows the corresponding eye diagrams of these data streams A and B and of the NOR gate output using both CR-SOAs and conventional SOAs. The Q-factor is a sensitive performance metric and is calculated for evaluating the performance of the target operation. The Q-factor is defined as $(P_1 - P_0)/(\sigma_1+\sigma_0)$ (Dutta and Wang 2013), where $P_{1,0}$ and $\sigma_{1,0}$ are the mean peak powers and standard deviations of binary outputs '1' and '0', respectively. This metric must be greater than 6 so that the associated bit error rate (BER), which is linked to the Q-factor by BER = $(2\pi)^{-1/2}$ exp[−0.5 Q-factor^2]/Q-factor (Thapa et al. 2019), is less than 10^{-9} for acceptable logic performance (Kotb and Guo 2020a, b). The Q-factor values obtained for the NOR logic gate at 120 Gb/s using CR-SOAs and conventional SOAs are 14 and 4.4, respectively. From this outcome, it is evident that a better performance is achieved for the NOR logic gate at 120 Gb/s when using the CR-SOAs, which is physically attributed to the presence of the CR layer that causes an ultrafast transition of carriers to the AR when the latter is

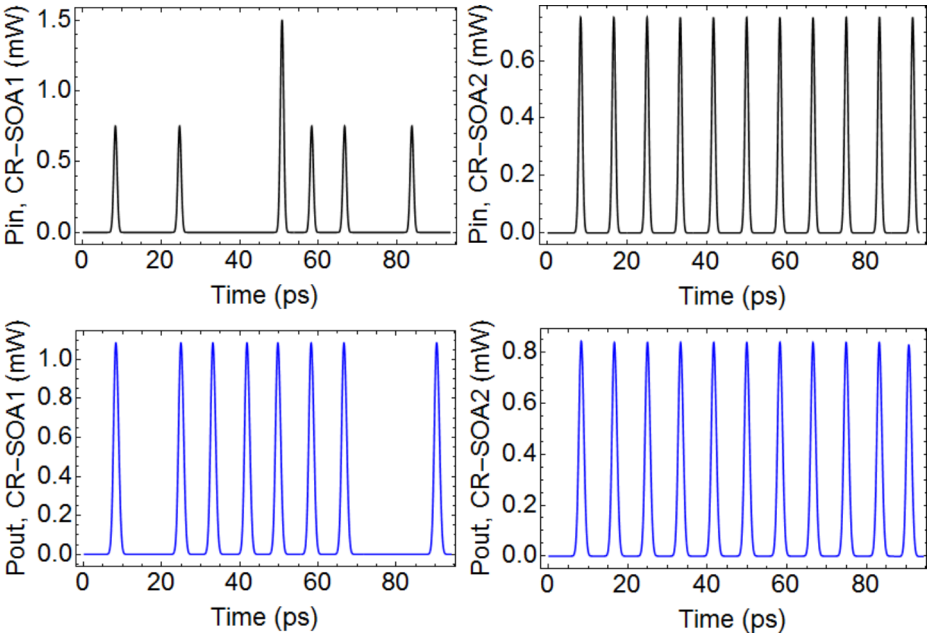

Fig. 4 Waveforms of input and output signals of CR-SOA1 and CR-SOA2 at 120 Gb/s

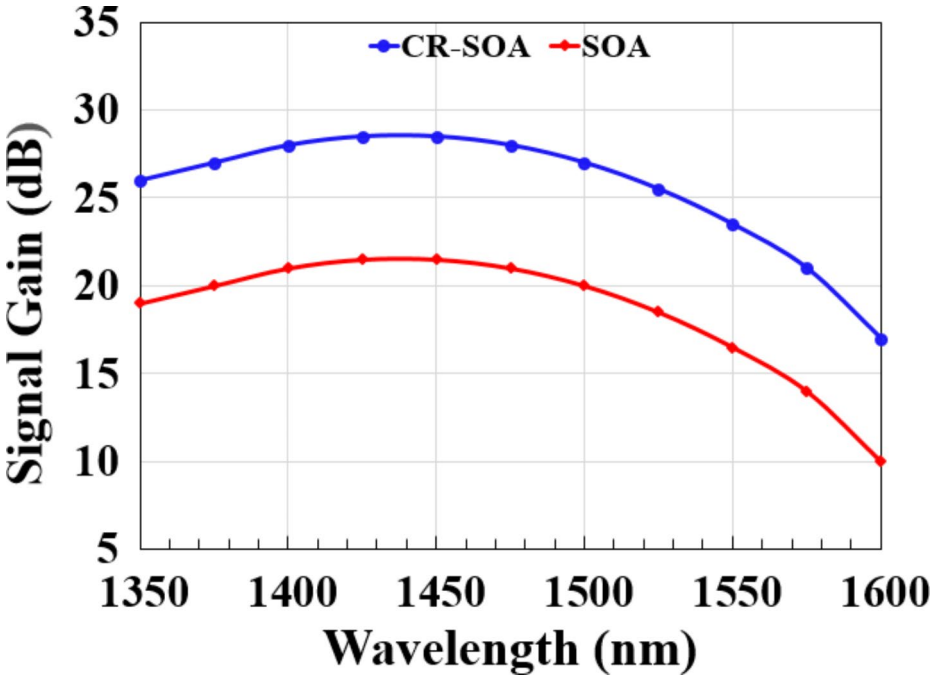

Fig. 5 Signal gain versus wavelength for CR-SOAs and SOAs

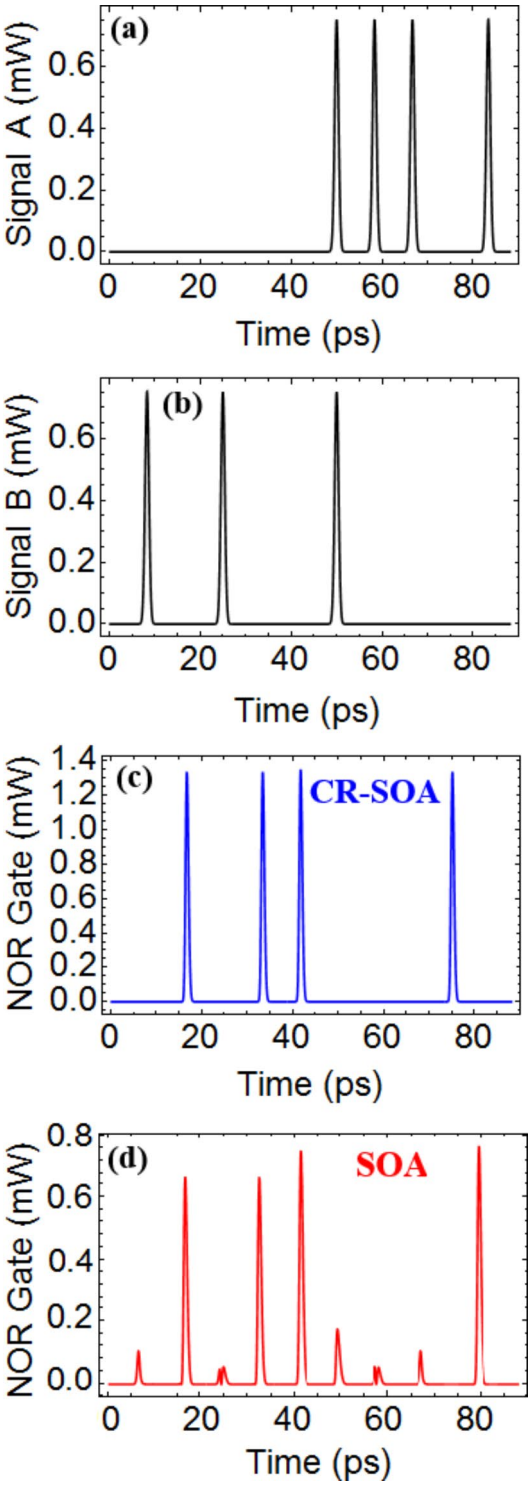

Fig. 6 AO NOR gate simulation results at 120 Gb/s. **(a)** Input signal A, **(b)** input signal B, **(c)** logic outcome using CR-SOAs-MZI, and (**d**) logic outcome using SOAs-MZI

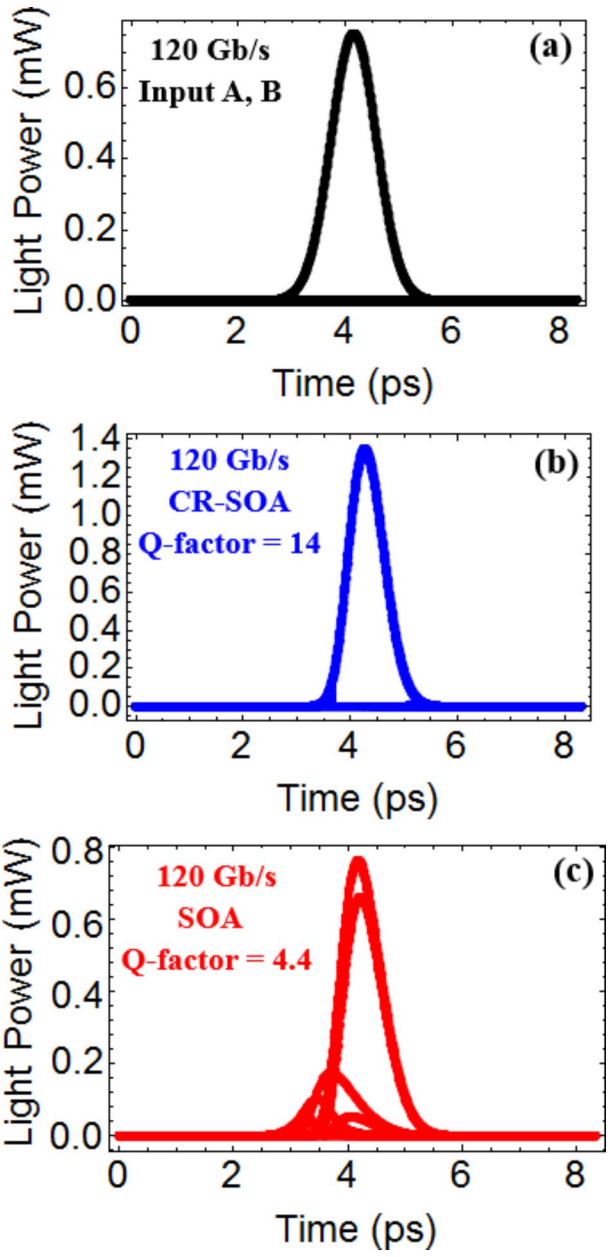

Fig. 7 AO NOR gate simulated eye diagrams at 120 Gb/s. (**a**) Input A, B, (**b**) output using CR-SOAs-MZI, and (**c**) output using SOAs-MZI

suitably depleted. In fact, the profile of the logic pulses is uniform, while the corresponding eye diagram is clear and open, when employing CR-SOAs. In contrast, logic pulses suffer from inadmissible intense peak-to-peak fluctuations, and the form of the corresponding eye diagram is strongly impaired, when using conventional SOAs.

We further examined the effects of the CW input power and injection bias current on the performance of the NOR logic gate at 120 Gb/s using both amplifiers, i.e. CR-SOAs- and

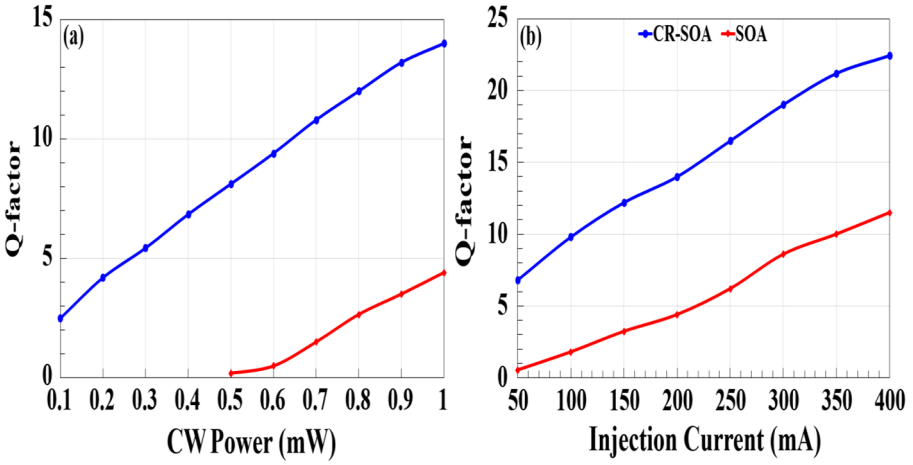

Fig. 8 Q-factor of logic NOR gate at 120 Gb/s versus **(a)** CW power and **(b)** injection current, for CR-SOAs and conventional SOAs

SOAs-MZI. As it can be seen in Fig. 8(a), the Q-factor is increased for higher CW power for both structures. This happens because the gain recovery time of both schemes is decreased with the increase of the CW power (Safari-Anzabi et al. 2021). This reflects positively on the quality of the NOR gate, and to a more pronounced extent for the CR-SOA whose gain response, as shown above, is additionally faster. Similarly, as shown in Fig. 8(b), the Q-factor is increased with the injection current for both CR-SOA- and SOA-based NOR gate at 120 Gb/s. A larger injection current provides more carriers to the AR, thereby allowing for faster gain recovery time and resulting in an increase of the Q-factor. From these results, it can also be observed that in the presence of the carrier reservoir, the Q-factor is higher even at lower CW powers or lower injection currents. For the conventional SOA case, applying high energetic pulses depletes strongly carriers, which need a longer time to be replenished to their initial level. For the CR-SOA, in turn, the carrier density recovers faster and is again available to be perturbed by an optical excitation (modulation signal) owing to the CR layer, which offers extra carriers to the depleted AR.

Figure 9 illustrates the Q-factor for the AO NOR gate utilizing both amplifiers, i.e. CR-SOAs- and SOAs-MZI at 120 Gb/s, versus the equivalent PRBS length (Siarkos et al. 2009). The whole PRBS sequence utilized in these systems scales to the power of 2, i.e. 2^n-1. The equivalent PRBS can suitably stress the operation of the considered logic gate as n increases, but the CR-SOAs-based scheme is tolerant and maintains an acceptable Q-factor value of 7.4 even at an equivalent PRBS length of 23. With the increase of n, the CR-SOAs-based NOR operation is further stressed, as the possibility of creating errors becomes higher due to the longer strings of '0's and '1's (Siarkos et al. 2009). This explains why the Q-factor is decreased as the PRBS order, n, is increased.

For the AO NOR operation employing CR-SOAs-based MZI at 120 Gb/s, the Q-factor versus the data and CW wavelengths is shown in Fig. 10. The wavelength range within which both signals should lie to ensure an acceptable Q-factor extends from 1510 nm to 1590 and thus is rather broad. This means that there is enough margin for selecting the

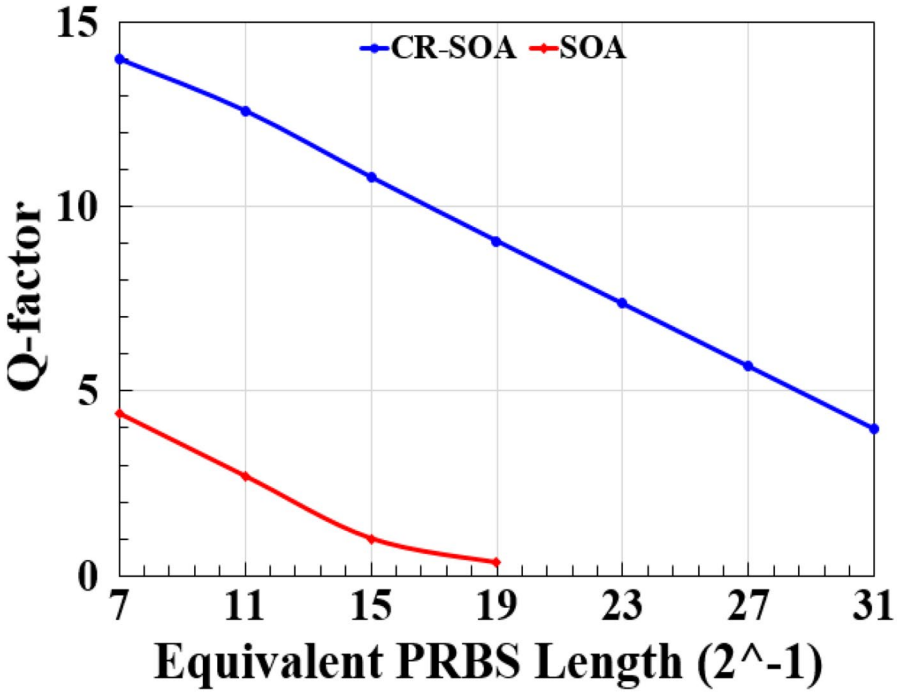

Fig. 9 Q-factor of logic NOR gate at 120 Gb/s versus equivalent PRBS length for CR-SOAs and conventional SOAs

spectral position and adjusting the detuning of these signals. This in turn relaxes the requirements for the laser sources used to generate them and for the optical filters employed to discriminate them, which is attractive from a practical perspective. This fact also ensures that all signals will spectrally lie within the specified CR-SOA bandwidth (see Fig. 5), as required for proper switching operation and subsequently for achieving the target AO logic operation.

In the previous results, the influence of the amplified spontaneous emission (ASE) on both amplifiers was neglected. However, since the main contribution of noise in SOAs is due to ASE. its effect on the logic performance should not be neglected. Therefore, the ASE power, which is given by $P_{ASE} = N_{SP} (G_0 - 1) 2\pi\hbar\upsilon B_0$ (Kotb 2013a, b; Kotb and Guo 2020a, b; Dutta and Wang 2013), is numerically added to the NOR output power given by Eq. (8). Then an increase in the ASE level shifts the mean value of '0' bits, thus resulting in an inevitable decrease of the Q-factor according to its definition. Still, the CR-SOA is tolerant to ASE, since the Q-factor remains acceptable at 6.8 even at an ASE power of 3.5 μW, while this is not possible when using the conventional SOA, as shown in Fig. 11(a). Moreover, it is useful to estimate at what speed the CR-SOA can operate while maintaining acceptable performance. This information is extracted from Fig. 11(b), which illustrates the Q-factor versus the operating data rate for both CR-SOAs- and SOAs-based NOR gate. From this diagram, it is noticed that the slow dynamic response of the conventional SOA impedes

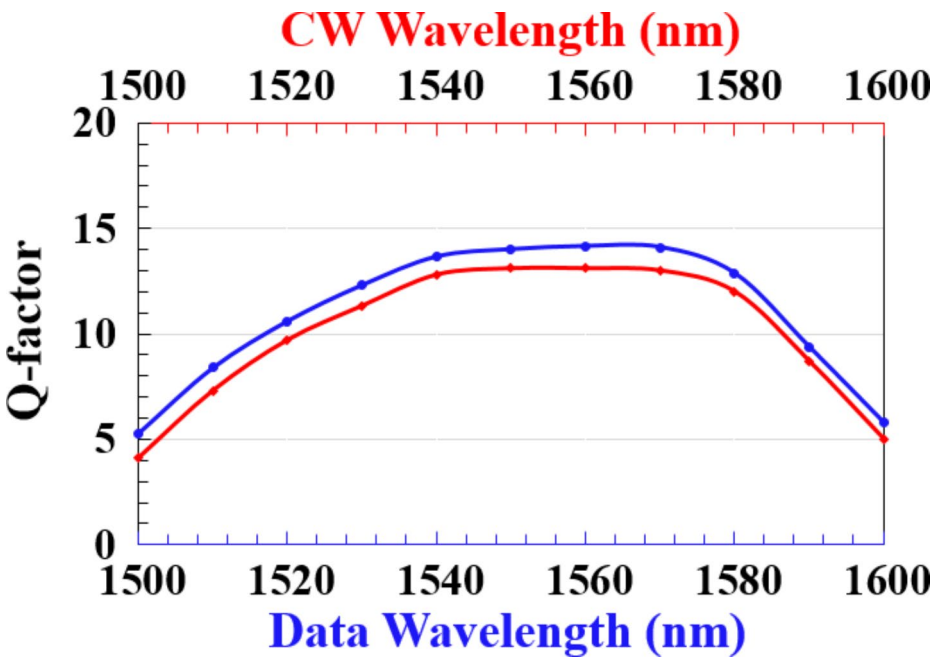

Fig. 10 Q-factor versus data wavelength (blue color) and CW wavelength (red color) using CR-SOAs-based MZI at 120 Gb/s

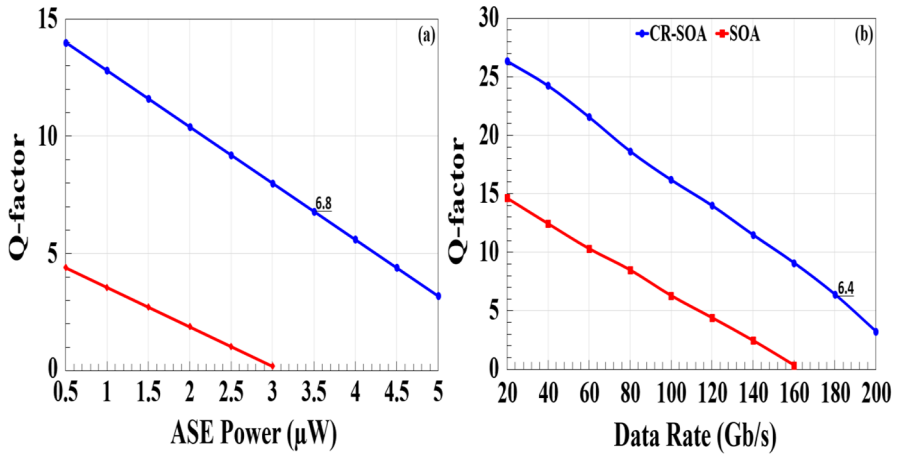

Fig. 11 Q-factor of logic NOR gate versus **(a)** amplified spontaneous emission (ASE) power and **(b)** operating data rate, for CR-SOAs and conventional SOAs

operation at rates above 100 Gb/s, as the Q-factor is strongly degraded, whereas the CR-SOA can operate up to 180 Gb/s with more than acceptable (=6.4) Q-factor.

Finally, to validate that the NOR gate based on CR-SOAs-MZI achieves high performance, we considered it in relation to other SOA-based schemes and data rates, as shown

Table 2 Comparison of NOR gate realizations for different SOAs-based schemes and data rates

Scheme	Data rate (Gb/s)	Q-factor	Ref.
SOA	40	8.8	(Sun et al. 2007)
	80	15.7	(Kotb et al. 2018)
	120	4.4	This work
CR-SOA	120	14	This work
PC-SOA	160	21.1	(Kotb and Guo 2020a, b)
SOA-TPA	250	12	(Kotb 2015)
QD-SOA	160	7	(Dimitriadou and Zoiros 2012)
	250	17.3	(Kotb 2013a, b)
	1000	40	(Kotb 2013a, b)
	2000	4.8	(Kotb and Guo 2020a, b)
QD-SOA-TPA	2000	9.6	(Kotb and Guo 2020a, b)

in Table 2. The Table highlights the merit of adopting the proposed CR-SOAs-MZI scheme for executing the NOR logic function at 120 Gb/ with a high Q-factor. The operating data rates can be further increased based on SOAs' technology while keeping logic performance acceptable by placing QDs in the SOA's active region (Kotb 2013a, b; Kotb and Guo 2020a, b; Dutta and Wang 2013), integrating photonic crystals (PCs) (Kotb and Guo 2020a, b), or exploiting the potential of nonlinear effects such as two-photon absorption (TPA) (Kotb 2015).

3 Conclusion

In this paper, we undertook the task of investigating the feasibility and assessing the performance, of an AO NOR logic gate at 120 Gb/s RZ-OOK data when using CR-SOAs in a MZI. By examining the Q-factor dependence on different critical operating factors, including ASE, a fair performance comparison was conducted between the CR-SOAs- and ordinary SOAs-assisted MZIs NOR gate schemes. The results showed that the NOR logic function can be executed correctly and with high quality using CR-SOAs, which is not possible when resorting to conventional SOAs. The simulations quantified this fact by the high Q-factor of 14 achieved in the former case, as opposed to the poor Q-factor of 4.4 in the latter case. This suggests that CR-SOAs can play an increasingly important role as nonlinear elements in the design and implementation of ultrafast AO circuits and subsystems of enhanced functionality.

Acknowledgements Amer Kotb appreciates the Chinese Academy of Sciences President's International Fellowship Initiative (Grant No. 2022VMB0013).

Funding The authors declare that no funds, grants, or other support were received during the preparation of this manuscript. The author has no relevant financial or non-financial interests to disclose.

Data Availability The datasets generated during and/or analyzed during the current study are available from the publications in the reference list and from the corresponding author.

Declarations

Conflict of interest All authors have declare that they have no conflict of interest.

References

Chan, L.Y., Qureshi, K.K., Wai, P.K.A., Moses, B., Lui, L.F.K., Tam, H.Y., Demokan, M.S.: All-optical bit-error monitoring system using cascaded inverted wavelength converter and optical NOR gate. IEEE Photon. Technol. Lett. 15, 593–595 (2003)

Dimitriadou, E., Zoiros, K.E.: Proposal for all-optical NOR gate using single quantum-dot semiconductor optical amplifier-based Mach–Zehnder interferometer. Opt. Commun. 285, 1710–1716 (2012)

Dutta, N.K., Wang, Q.: Semiconductor Optical Amplifiers, 2nd edn. World Scientific Publishing Company, Singapore (2013)

El-Saeed, E.M., El-Aziz, A., Fayed, A., Aly, H.A.: Optical logic gates based on semiconductor optical amplifier Mach–Zehnder interferometer: design and simulation. Opt. Eng. 55, 025104 (2016)

Jung, Y.J., Son, C.W., Jhon, Y.M., Lee, S., Park, N.: One-level simplification method for all-optical combinational logic circuits. IEEE Photon. Technol. Lett. 20, 800–802 (2008)

Kotb, A.: NOR gate based on QD-SOA at 250 Gbit/s. Opt. Quantum Electron. 45, 473–480 (2013a)

Kotb, A.: 1 Tb/s high-quality factor NOR gate based on quantum-dot semiconductor optical amplifier. Opt. Quantum Electron. 45, 1258–1268 (2013b)

Kotb, A.: Simulation of all-optical logic NOR gate based on two-photon absorption with semiconductor optical amplifier-assisted Mach-Zehnder interferometer with the effect of amplified spontaneous emission. Korean J. Phys. Soc. 66, 1593–1598 (2015)

Kotb, A., Zoiros, K.E., Guo, C.: All-optical XOR, NOR, and NAND logic functions with parallel semiconductor optical amplifier-based Mach-Zehnder interferometer modules. Opt. Laser Technol. 108, 426–433 (2018)

Kotb, A., Guo, C.: Numerical modeling of photonic crystal semiconductor optical amplifiers-based 160 Gb/s all-optical NOR and XNOR logic gate. Opt. Quantum Electron. 52, 89 (2020a)

Kotb, A., Guo, C.: All-optical NOR and XNOR gates at 2 Tb/s based on two-photon absorption in quantum-dot semiconductor optical amplifiers. Opt. Quantum Electron. 52, 30 (2020b)

Kotb, A.: Ultrafast carrier reservoir semiconductor optical amplifiers-based all-optical AND logic gate. Opt. Eng. 60, 026104 (2021)

Kotb, A., Zoiros, K.E., Li, W.: Numerical Study of carrier reservoir semiconductor optical amplifier-based all-optical XOR logic gate. J. Mod. Opt. 68, 161–168 (2021a)

Kotb, A., Zoiros, K.E., Li, W.: Execution of all-optical Boolean OR logic using carrier reservoir semiconductor optical amplifier-assisted delayed interferometer. Opt. Laser Technol. 142, 107230 (2021b)

Kotb, A., Zoiros, K.E., Li, W.: Realization of ultrafast all-optical NAND and XNOR logic functions using carrier reservoir semiconductor optical amplifiers. J. Supercomp. 77, 14617–14629 (2021c)

Mehra, R., Jaiswal, S., Dixit, H.K., Singh, P.: Performance analysis of all-optical NOR gate at 80 Gb/s. Optik. 124, 1672–1675 (2013)

Safari-Anzabi, K., Habibzadeh-Sharif, A., Connelly, M.J., Rostami, A.: Performance enhancement of an all-optical XOR gate using quantum-dot based reflective semiconductor optical amplifiers in a folded Mach-Zehnder interferometer. Opt. Laser Technol. 135, 106628 (2021)

Scaffardi, M., Andriolli, N., Meloni, G., Berrettini, G., Fresi, F., Castoldi, P., Potì, L., Bogoni, A.: Photonic combinatorial network for contention management in 160 Gb/s-interconnection networks based on all-optical 2×2 switching elements. IEEE J. Sel. Top. Quantum Electron. 13, 1531–1539 (2007)

Siarkos, T., Zoiros, K.E., Nastou, D.: On the feasibility of full pattern-operated all-optical XOR gate with single semiconductor optical amplifier-based ultrafast nonlinear interferometer. Opt. Commun. 282, 2729–2740 (2009)

Sun, H., Chen, Z., Ma, S., Dutta, N.K.: All-optical logic NOR gate at 40 Gb/s using SOA-based Mach-Zehnder interferometer. Proc. SPIE 6775, 67750F (2007)

Thapa, S., Zhang, X., Dutta, N.K.: Effects of two-photon absorption on pseudo-random bit sequence operating at high speed. J. Mod. Opt. 66, 100–108 (2019)

Xu, J., Zhang, X., Liu, D., Huang, D.: Ultrafast all-optical NOR gate based on semiconductor optical amplifier and fiber delay interferometer. Opt. Express. 14, 10708–10714 (2006)

Xu, J., Zhang, X., Dong, J., Liu, D., Huang, D.: Simultaneous all-optical AND and NOR gates for NRZ differential phase-shift-keying signals. IEEE Photon. Technol. Lett. 20, 596–598 (2008)

Publisher's Note Springer Nature remains neutral with regard to jurisdictional claims in published maps and institutional affiliations.

Springer Nature or its licensor holds exclusive rights to this article under a publishing agreement with the author(s) or other rightsholder(s); author self-archiving of the accepted manuscript version of this article is solely governed by the terms of such publishing agreement and applicable law.